LETTER

Vector vortices with tunable polarization states directly generated in a microchip laser

Applied Physics Express 12, 052012 (2019)
https://doi.org/10.7567/1882-0786/ab1558

LETTER

Vector vortices with tunable polarization states directly generated in a microchip laser

Dimeng Chen, Xiaocan Wang, Hongsen He, and Jun Dong*

Laboratory of Laser and Applied Photonics (LLAP), Department of Electronic Engineering, School of Electronic Science and Engineering, Xiamen University, Xiamen 361005, People's Republic of China

*E-mail: jdong@xmu.edu.cn

Received February 28, 2019; revised March 26, 2019; accepted April 2, 2019; published online April 15, 2019

High beam quality vector vortices with tunable polarization states have been produced in a Yb:YAG microchip laser under focused annular beam pumping. Radial, anti-radial, and hybrid polarization are obtained in vector vortices by adjusting the offset distance (Δz) between the focus spot and the Yb:YAG crystal. Output powers of over 1 W for vector vortices with three polarization states are achieved within a wide range of Δz (e.g., 1.25 mm). The efficient, high-power Yb:YAG microchip laser is demonstrated to generate vector vortices with an output power of 1.7 W and an optical efficiency of 22%. © 2019 The Japan Society of Applied Physics

Supplementary material for this article is available online

Vector vortex beams have potential applications in optical trapping, material processing, quantum information processing, high-resolution spectroscopy, and so on, owing to their unique characteristics of a doughnut-shaped transverse intensity distribution, helical phase, and having orbital angular momentum (OAM).[1] Inhomogeneous polarization states of the vector vortex beams are an important property besides amplitude and phase.[2] Because of their unique polarization properties, vector vortex lasers have been widely used in various applications. Sharper focal spots have been achieved in a radially polarized laser with a high numerical aperture lens,[3] and a hollow dark spot has been obtained by focusing an azimuthally polarized vortex beam. Focusing a double-mode vortex laser consisting of radial and azimuthal polarization has been used to form an optical plate or a three-dimensional optical cage.[4] Besides radially and azimuthally polarized vortex beams, other polarization states have been predicted theoretically and demonstrated experimentally by superposition of two orthogonal linearly polarized Laguerre–Gauss lasers;[5] complex flower patterns have been formed by tightly focusing such beams with a high numerical aperture lens.[6] Vector vortex lasers are usually generated by passing a Gaussian beam through specific phase plates such as a spatial light modulator,[7] q-plate,[8] or digital micromirror device.[9] Direct generation of radially or azimuthally polarized vortex beams has been achieved in a laser resonator by applying mode-selecting elements inside the cavity, such as birefringent elements,[10,11] conical Brewster prisms,[12] or polarization-selective end mirror devices.[13] Interferometers have been used to generate vector vortex beams by combining two orthogonal linearly polarized HG_{01} modes.[5,14] Annular pump beams have been used to end-pump solid-state lasers for vector vortex beam generation. Various methods such as mode conversion fibers,[15] axicons,[16] and hollow focus lenses[17] have been developed to realize annular-shaped pump beams. Radially and azimuthally polarized vector vortex lasers have been generated in annular beam-pumped Nd:YAG or Nd:YVO_4 solid-state lasers by adjusting the incident pump power or misaligning the cavity.[17] However, manipulation of polarization states in solid-state lasers is a major challenge. The efficiency of vector vortex lasers with Nd^{3+}-doped laser materials as gain media is low owing to the low quantum efficiency and severe thermal effects. Compared to Nd^{3+}-doped laser materials, ytterbium ion (Yb^{3+})-doped laser materials, especially Yb:YAG, are ideal candidates as solid-state laser materials for achieving vector vortex lasers with high power and high efficiency since they have remarkable properties such as low quantum defects, broad absorption and emission spectra, and high doping concentration.[18,19]

In this letter, radially, hybrid, and anti-radially polarized vector vortices have been obtained by controlling the absorbed pump power distribution in a Yb:YAG microchip laser. Output powers of over 1 W have been achieved for three polarized vector vortex lasers. The effect of the offset distance (Δz) between the focus spot and the Yb:YAG crystal on the polarization states of vector vortices has been studied experimentally.

The focused annular pump beam from a fiber-coupled laser diode can be approximated as a superposition of TEM_{00} modes with a z-dependent separation of r_0, and the normalized pump power distribution is

$$R_p(r,z)=\frac{\alpha}{\pi w_p^2(z)}\frac{\exp(-\alpha z)}{[1-\exp(-\alpha l)]}\left[\exp\left(\frac{-2(r-r_0)^2}{w_p^2(z)}\right)+\exp\left(\frac{-2(r+r_0)^2}{w_p^2(z)}\right)\right] \quad (1)$$

where α is the absorption coefficient of the Yb:YAG crystal at the pump wavelength, l is the length of the Yb:YAG crystal, $w_p(z)$ is the beam radius of the TEM_{00} mode at position z along the beam propagation direction, r_0 is the distance between the beam axis and the position of the TEM_{00} mode at the maximum intensity, and can be expressed as $r_0=|z-z_0|\tan(\theta_p)$, θ_p is the far-field half-angle, and z_0 is the focal spot position.

$LG_{0,1}$ mode oscillation is preferable in a microchip laser under annular beam pumping because good mode overlap is achieved between the laser and pump beams. For an annular beam end-pumped Yb:YAG microchip laser, the threshold pump power P_{th} required for a single $LG_{0,1}$ mode oscillation, taking account into the reabsorption loss of the Yb:YAG crystal,[20] can be expressed as[21,22]

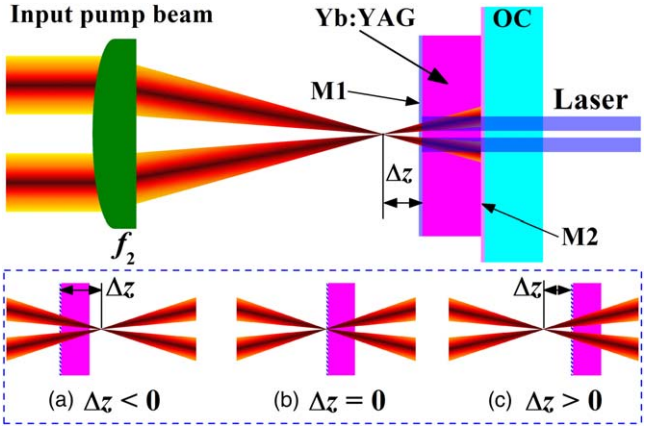

Fig. 1. (Color online) Schematic of a focused annular beam-pumped Yb:YAG microchip laser for generating $LG_{0,1}$ vortices with tunable polarization states. f_2 is the focus lens, M1 is the rear cavity mirror, M2 is the front cavity mirror, and OC is the output coupler. The inset illustrates the three cases of relative offset between the end surface of the Yb:YAG crystal and the focal spot (Δz).

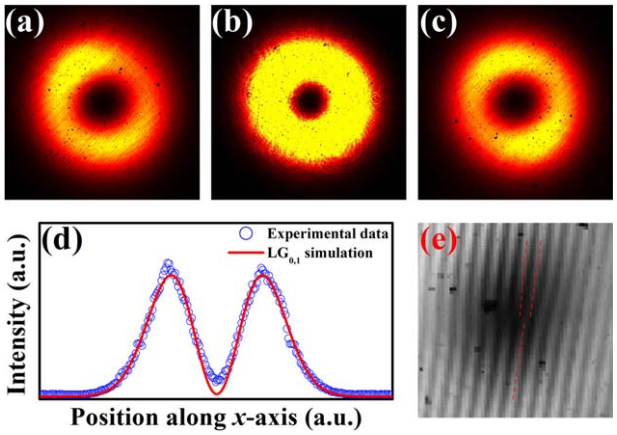

Fig. 2. (Color online) Intensity profiles of experimentally obtained $LG_{0,1}$ vortices at (a) $\Delta z = -0.5$ mm, (b) $\Delta z = -0.2$ mm, (c) $\Delta z = 0$ mm. (d) Transverse intensity profile of the $LG_{0,1}$ vortex along the x-axis; the solid line is the theoretical fit with the $LG_{0,1}$ expression. (e) Interference pattern of the $LG_{0,1}$ vortex beam with a plane-wave reference beam; the dashed lines show the fringes at the fork dislocation.

$$P_{\text{th}} = \frac{h\nu_p(L_i + T + 2N_1^0\sigma l)}{2\sigma l\tau\eta_a} \frac{1}{\iiint s_{01}(r,\phi,z)R_p(r,z)dV} \quad (2)$$

where τ and σ are the fluorescence lifetime and emission cross section of Yb:YAG crystal, L_i is the intrinsic cavity loss, T is the transmission of the cavity mirrors, $2N_1{}^0\sigma l$ is the saturable reabsorption loss of a quasi-four-level Yb:YAG crystal, $\Delta N^0 = N_2{}^0 - N_1{}^0 \approx -N_1{}^0 = -f_1 N_0$ is the unpumped population-inversion density, f_1 is the fractional factor of the lower laser level, N_0 is the doping concentration of Yb^{3+} ions, l is the length of the Yb:YAG crystal, η_a is the absorption efficiency, h is the Planck constant, ν_p is the pump frequency, and $s_{01}(r, \phi, z)$ is the normalized intracavity $LG_{0,1}$ mode intensity distribution.

Figure 1 depicts a schematic of a focused annular beam-pumped Yb:YAG microchip laser for generating polarization-tunable vector vortices. The pump source was a fiber-coupled laser diode with ring-shaped intensity distribution profile. The annular beam from fiber was collimated and focused with two identical lenses (focal length 8 mm). The beam diameter at focal spot was measured to be 40 μm and the beam divergence angle was about 10°. The gain medium was a Yb:YAG crystal (1.2 mm thick, 10 at% Yb^{3+} ion doping concentration). A high reflection coating at 1000–1100 nm was applied at one surface of the Yb:YAG crystal to work as the rear cavity mirror (M1). Partial reflection coating of 85% at 1000–1100 nm on plane-parallel glass acted as the front cavity mirror (M2). The offset distance, Δz, between the end surface of the Yb:YAG crystal and the focal spot is a key parameter for controlling the polarization states of vector vortices; Δz was varied by moving the laser head along the pump beam propagation direction. As shown in Figs. 1(a)–1(c), $\Delta z = 0$ indicates the focal spot located just on the end surface of the Yb:YAG crystal; $\Delta z < 0$ indicates that the end surface is close to the focus lens; $\Delta z > 0$ indicates that the end surface is away from the focus lens.

The output transverse intensity profiles at different Δz and incident pump power (P_{in}) were measured with a beam profile analyzer. Figures 2(a)–2(c) show the measured intensity profiles of optical vortices generated at $P_{\text{in}} = 6.1$ W. These profiles at different Δz retain nearly null intensity along the beam axis, and are all typically doughnut-shaped. As shown in Fig. 2(d), the experimentally obtained transverse profile along the x-axis is well fitted by the $LG_{0,1}$ expression, which is clear evidence for the $LG_{0,1}$ mode being generated in the microchip laser. The phase of the obtained $LG_{0,1}$ modes was checked by interference with a plane-wave reference beam. One interference fringe splits into two at a fork-like dislocation, as shown in Fig. 2(e), which clearly shows that the $LG_{0,1}$ doughnut-shaped beams are optical vortices with helical wave-fronts and a topological charge of 1. The helical phases of the optical vortices suggest that such vortex beams possess OAM. The vortex laser beam quality was also evaluated by measuring the position-dependent laser beam waists along the beam propagation direction. The beam quality factor (M^2) of the output vortex lasers at $P_{\text{in}} = 7.8$ W was measured to be <2.4, which is close to the theoretically calculated value of 2 for an ideal first-order $LG_{0,1}$ mode.

The polarization states of the optical vortices were checked by passing the vortex beams through a linear polarizer. Interestingly, three polarization states were observed, depending on Δz. A radial polarization (RP) state was obtained when Δz was less than -0.3 mm. An anti-radial polarization (ARP) state was observed when Δz was larger than -0.1 mm. A hybrid polarization (HP) state, combining RP and ARP, was observed when Δz was within the range from -0.3 mm to -0.1 mm. The measured polarization patterns at different rotation angles after passing through a linear polarizer for three polarized vector vortices at $\Delta z = -0.5$ mm, -0.2 mm, and 0 mm are shown in Fig. 3. For the RP vortex beam shown in Fig. 3(a), a two-lobe pattern was obtained after transmission through a linear polarizer. The two-lobe pattern rotated in the same direction upon rotating the linear polarizer, as shown in Visualization 1. For the ARP vortex beam shown in Fig. 3(c), a two-lobe pattern was also obtained after passing through the linear polarizer; however, the pattern rotated in the opposite direction upon rotating the linear polarizer, as shown in Visualization 3. For the HP vortex beam shown in Fig. 3(b), as shown in Visualization

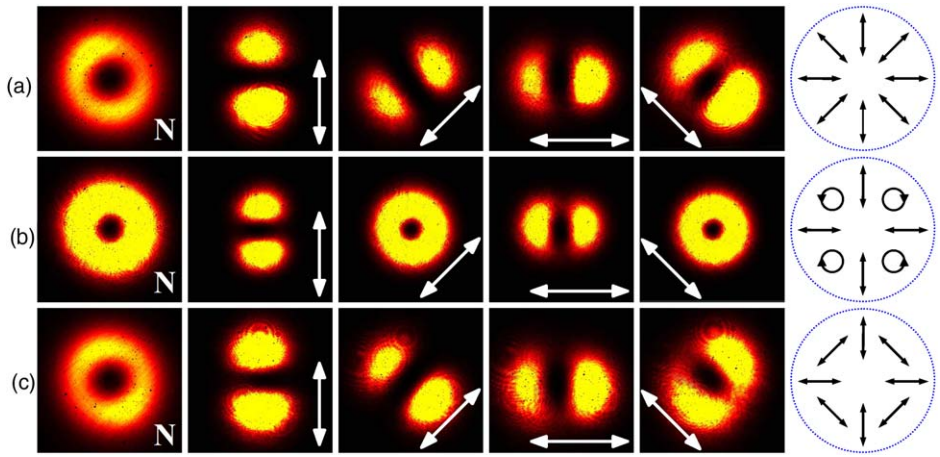

Fig. 3. (Color online) Polarization patterns of $LG_{0,1}$ vector vortices for (a) RP at $\Delta z = -0.5$ mm, (b) HP at $\Delta z = -0.2$ mm, and (c) ARP at $\Delta z = 0$ mm. The arrows show the directions of the linear polarizer. "N" indicates the original vector vortices. An illustration of the polarization states RP, HP, and ARP is also given in the figure (see Visualization 1 for AR, Visualization 2 for HP, and Visualization 3 for ARP). See the supplementary data, available online at stacks.iop.org/APEX/12/052012/mmedia.

2, the two-lobe pattern was observed parallel to the linear polarizer when the latter was along the vertical direction. The two-lobe pattern changed to a doughnut profile when the linear polarizer was rotated 45°. When it was rotated along the horizontal direction, the doughnut profile changed to a two-lobe pattern along the horizontal direction. When the linear polarizer was further rotated 45°, the two-lobe pattern along the horizontal direction changed to a doughnut profile. The transition among the polarization states of the vortex beams is reversible and can be easily tuned by adjusting Δz. The RP vortex beams are attributed to the preferential oscillation of the local linearly polarized beam along the radial direction compared to its counterpart component of the azimuthally polarized beam in the annular pumped Yb:YAG microchip laser.[17] The ARP vortex beams generated at $\Delta z > -0.1$ mm are due to the change of the Gouy phase of π induced by the tightly focused pump beam.[23] The combined effect of the Gouy phase before and after the focal spot determines the HP state of the vortex beams generated at $-0.3 < \Delta z < -0.1$ mm.

Figure 4 shows the measured output powers of the polarization-tunable vector vortex lasers at different Δz when P_{in} is set at 6.5 W. The maximum output power of 1.25 W is obtained at $\Delta z = -0.2$ mm. When Δz changes from -0.2 mm, the output power decreases, and the laser does not oscillate at $\Delta z = -1.7$ mm and 1.8 mm. The output power drops faster with $|\Delta z|$ for $\Delta z < -0.8$ mm than for $\Delta z > 0.4$ mm. The variation of Δz for the ARP oscillation is wider than that for the RP oscillation. The output power for the HP vortex laser is almost unchanged for Δz from -0.3 to -0.1 mm. An output power of over 1 W for vector vortex lasers with three polarization states is obtained over a wide tunable range of 1.25 mm for Δz (e.g. from -0.85 mm to -0.3 mm for the RP vortex laser; from -0.3 to -0.1 mm for the HP vortex laser; from -0.1 mm to 0.4 mm for the ARP vortex laser). Therefore, high-power, polarization-tunable vector vortex lasers with OAM have been demonstrated by simply adjusting Δz. The threshold pump power (P_{th}) of vector vortex lasers at different Δz was measured by moving the Yb:YAG crystal along the pump beam propagation direction. The dependence of P_{th} on Δz is also plotted in Fig. 4. The lowest P_{th} was about 1.72 W for Δz from

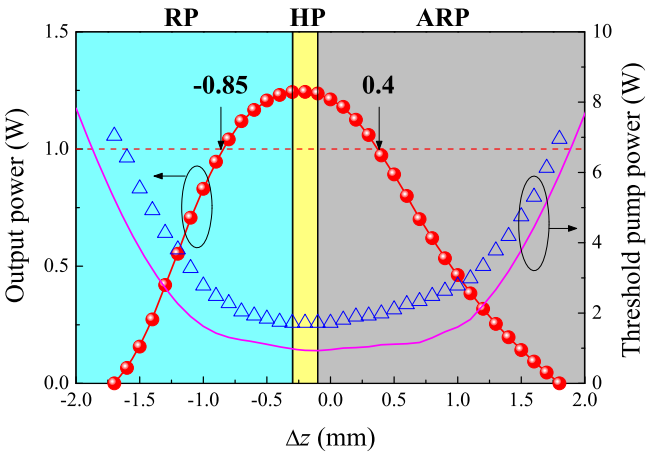

Fig. 4. (Color online) Output power of vector vortex lasers as a function of Δz when P_{in} is 6.5 W. The threshold pump powers for vector vortex lasers at different Δz are also given. The solid line is the theoretically calculated threshold pump power at different Δz. The dashed line indicates the 1 W output power.

-0.4 mm to 0. P_{th} increases faster with $|\Delta z|$ for $\Delta z < -0.6$ mm than for $\Delta z > 0.4$ mm. The asymmetrical variation of the output power and P_{th} with Δz is caused by mode matching between the pump and laser beams, which is induced by the asymmetrical absorbed pump power distribution along the crystal length. The increase of P_{th} with $|\Delta z|$ at $|\Delta z| > 0.5$ mm is due to a decrease of the pump power intensity, which is induced by enlarging the annular pump beam area when the Yb:YAG crystal is moved far away from focal spot. Therefore, more pump power is required to overcome the lasing threshold. When the parameters of the focused annular beam end-pumped Yb:YAG microchip laser are $w_{p0} = 20\ \mu$m, $\theta_p = 10°$, $L_i = 0.01$, $T = 0.15$, $\alpha = 10\ \text{cm}^{-1}$, $N_0 = 1.38 \times 10^{21}\ \text{ions cm}^{-3}$, $f_1 = 0.046$, $l = 1.2$ mm, $\nu_p = 3.2 \times 10^{14}$ Hz, $\eta_a = 1\text{-exp}(-\alpha l)$, and $w_l = 100\ \mu$m, the threshold pump powers for $LG_{0,1}$ modes at different Δz are calculated with Eq. (2). The variation of theoretically calculated threshold pump power with Δz is also shown in Fig. 4, and is in fair agreement with the experimental results. The theoretically calculated P_{th} at different Δz are lower than the experimental values, which is attributed to inaccurate estimation of the intracavity losses in the theoretical

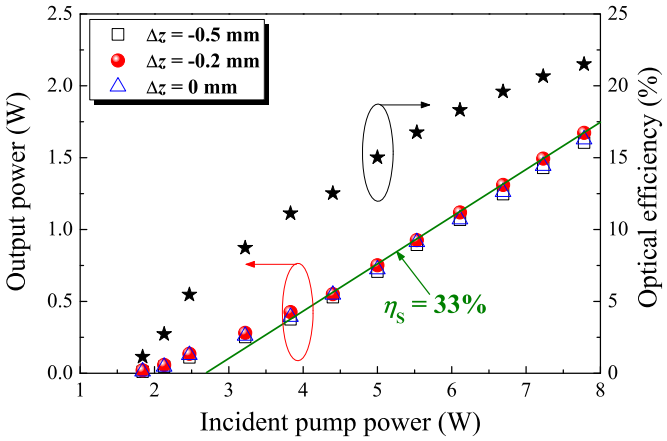

Fig. 5. (Color online) Output power as a function of P_{in} at $\Delta z = -0.5$ mm, -0.2 mm, and 0 mm. Variation of the optical efficiency with P_{in} for $\Delta z = -0.2$ mm is also given. The solid line is the linear fit of the output power with P_{in} at $\Delta z = -0.2$ mm.

calculations. Also, the pump power-dependent thermal effect of the gain medium is not considered in the theoretical calculation. This effect changes the optical properties of the Yb:YAG crystal, such as broadening the optical spectra and decreasing the absorption coefficient and emission cross section,[18] which have a great effect on the laser threshold.

Figure 5 shows the output power of the three polarized vortex lasers (RP, HP, and ARP) as a function of P_{in} at $\Delta z = -0.5$ mm, -0.2 mm, and 0 mm, respectively. The P_{th} values for the three lasers are comparable. The output power increases slowly with P_{in} below 4 W, and then increases rapidly and linearly with P_{in} above 4 W. The HP vortex laser exhibits better performance compared to the RP and ARP lasers owing to excellent mode matching between the pump and laser beams when Δz is between -0.3 and -0.1 mm. The slope efficiency of the HP vortex laser is 33%. An output power of 1.7 W is obtained at $P_{in} = 7.8$ W, and the corresponding optical efficiency is about 22%, so efficient performance has been demonstrated in a polarization-tunable vector vortex Yb:YAG microchip laser.

In conclusion, high beam quality vector vortex lasers with tunable polarization states have been demonstrated in an annular beam-pumped Yb:YAG microchip laser. The transition among the polarization states (RP, HP and ARP) of the vector vortex beams has been manipulated by controlling the Δz-dependent absorbed pump power distribution inside the Yb:YAG crystal. Output powers of over 1 W have been obtained for vector vortex lasers with different polarization states. Highly efficient laser performance with an optical efficiency of over 22% and output power of 1.7 W has been achieved for the HP vortex laser. Monolithic vector vortex lasers with flexible polarization have potential applications in materials processing, optical trapping, quantum information processing, among others.

Acknowledgments This work was supported by the National Natural Science Foundation of China (61275143, 61475130), and the Program for New Century Excellent Talents in University (NCET-09-0669).

ORCID iDs Jun Dong https://orcid.org/0000-0001-7072-5435

1) Q. W. Zhan, Adv. Opt. Photonics **1**, 1 (2009).
2) Z. Y. Chen, L. M. Hua, and J. X. Pu, in *Progress in Optics*, ed. E. Wolf, (Elsevier, Amterdam, 2012) Vol. 57, p. 219.
3) R. Dorn, S. Quabis, and G. Leuchs, Phys. Rev. Lett. **91**, 233901 (2003).
4) X. L. Wang, J. P. Ding, J. Q. Qin, J. Chen, Y. X. Fan, and H. T. Wang, Opt. Commun. **282**, 3421 (2009).
5) C. Maurer, A. Jesacher, S. Fürhapter, S. Bernet, and M. Ritsch-Marte, New J. Phys. **9**, 78 (2007).
6) M. Rashid, O. M. Marago, and P. H. Jones, J. Opt. A-Pure Appl. Opt. **11**, 065204 (2009).
7) S. Mamani, E. Bendau, J. Secor, S. Ashrafi, J. J. Tu, and R. R. Alfano, Appl. Optics **56**, 2171 (2017).
8) F. Cardano, E. Karimi, S. Slussarenko, L. Marrucci, C. de Lisio, and E. Santamato, Appl. Optics **51**, C1 (2012).
9) Y. X. Ren, R. D. Lu, and L. Gong, Ann. Phys.-Berlin **527**, 447 (2015).
10) K. Yonezawa, Y. Kozawa, and S. Sato, Jpn. J. Appl. Phys. Part 1 - Regul. Pap. Brief Commun. Rev. Pap. **46**, 5160 (2007).
11) S. N. Khonina, S. V. Karpeev, S. V. Alferov, and V. A. Soifer, J. Opt. **17**, 065001 (2015).
12) Y. Kozawa and S. Sato, Opt. Lett. **30**, 3063 (2005).
13) M. A. Ahmed, A. Voss, M. M. Vogel, and T. Graf, Opt. Lett. **32**, 3272 (2007).
14) M. Padgett, J. Arlt, N. Simpson, and L. Allen, Am. J. Phys. **64**, 77 (1996).
15) Z. Q. Fang, K. G. Xia, Y. Yao, and J. L. Li, Appl. Phys. B-Lasers Opt. **117**, 219 (2014).
16) M. D. Wei, Y. S. Lai, and K. C. Chang, Opt. Lett. **38**, 2443 (2013).
17) H. S. He, Z. Chen, and J. Dong, Appl. Phys. Express **10**, 052701 (2017).
18) J. Dong, M. Bass, Y. L. Mao, P. Z. Deng, and F. X. Gan, J. Opt. Soc. Am. B-Opt. Phys. **20**, 1975 (2003).
19) J. Dong, A. Shirakawa, K. Ueda, H. Yagi, T. Yanagitani, and A. A. Kaminskii, Appl. Phys. Lett. **89**, 091114 (2006).
20) W. P. Kong, A. Sugita, and T. Taira, Opt. Lett. **37**, 2661 (2012).
21) K. Kubodera, K. Otsuka, and S. Miyazawa, Appl. Optics **18**, 884 (1979).
22) T. Taira, W. M. Tulloch, and R. L. Byer, Appl. Optics **36**, 1867 (1997).
23) D. Kawase, Y. Miyamoto, M. Takeda, K. Sasaki, and S. Takeuchi, Phys. Rev. Lett. **101**, 050501 (2008).